Mathematics in Applied Sciences and Engineering
Volume **5**, Number **4**, December **2024**, pp.**276-291**
https://ojs.lib.uwo.ca/mase
https://doi.org/10.5206/mase/18033

INCORPORATING MEAN-FIELD VELOCITY DIFFERENCE IN A CONTINUUM MACROSCOPIC TRAFFIC FLOW MODEL FOR ADVERSE ROAD CONDITIONS

GABRIEL OBED FOSU, DICKSON ANOKYE, ALBERT ADU-SACKEY, AND BRIGHT EMMANUEL OWUSU

Abstract. In developing countries, the quality of driving infrastructure, specifically road conditions, is often suboptimal, presenting challenges and limitations for motorists. However, current traffic flow models have limitations in addressing problems caused by poor road networks. To address this issue, a new macroscopic traffic flow model has been proposed in this study that considers mean-field velocity differences on roads with suboptimal conditions. A thorough model derivation of this new macroscopic traffic flow model is presented. The study establishes crucial stability conditions, providing profound insights into traffic dynamics across diverse scenarios. Numerical simulations are presented to demonstrate the model's ability to capture shock waves, rarefaction waves, and local cluster effects. The study results offer new insights into traffic dynamics in adverse road conditions and enforce the need to enhance road infrastructure to alleviate congestion and enhance road safety.

1. Introduction

Traffic congestion is a widespread problem in today's cities, causing longer travel times, more fuel use, and increased pollution [39, 42, 49]. While existing traffic flow models [2, 18, 37, 38] have been useful in understanding and addressing congestion, they often struggle to handle the complexities of poor road networks. In this study, we aim to create a comprehensive traffic flow model that considers the mean-field velocity differences on road infrastructure having divots and craters.

Over the years, the transportation industry has seen significant progress and growth in terms of infrastructure, technology, and services. This has led to a revolution in travel, enabling people to move more efficiently and effectively between places, increasing productivity, and contributing to economic growth. However, this progress has come at a cost, with several negative consequences such as traffic congestion, and environmental concerns. Traffic congestion is a major social hazard that has emerged as a result of the rapid growth of the transportation industry. The increasing number of vehicles on the road has led to a rise in traffic jams, which can lead to delays, frustration, and reduced productivity. Additionally, traffic congestion has also been linked to increased air pollution, which can have adverse effects on human health. The increase in the number of vehicles on the road has led to increased emissions of greenhouse gases, contributing to global climate change.

To tackle these problems, researchers are closely studying various aspects of traffic, including how cars follow each other, patterns of starting and stopping, mysterious traffic jams that seem to appear out of nowhere, and the ebb and flow of traffic over time. By gaining a deeper understanding of these phenomena, researchers aim to come up with effective strategies and solutions to reduce the negative impacts associated with transportation, such as congestion and environmental issues.

With the increasing traffic challenges faced by modern cities, scholars have been actively researching various traffic flow models to address this issue. These models include car-following models [4, 5, 8,

Received by the editors 20 March 2024; accepted 11 November 2024; published online 24 November 2024.
2020 *Mathematics Subject Classification.* 35Q35, 65M06, 35L40, 76L05.
Key words and phrases. Vehicular Traffic Flow, LWR model, Dynamic Velocity Equation, Potholes, Mean-Field Speed.

28, 29, 30, 34, 35], which describe how drivers adjust their speed based on the distance from the car in front of them, and cellular automation models [3, 17, 20, 26, 31, 48], which simulate individual vehicle movements through a grid-like system. Other models include hydrodynamic models [6, 15, 40], which treat traffic flow as a fluid and use equations similar to those used in fluid mechanics to describe the movement of vehicles, and continuum models [1, 11, 12, 16, 38, 44, 45, 46, 51], which treat traffic flow as a continuous field rather than individual vehicles.

Among these models, one of the most foundational is the traffic wave theory, which was first introduced by Lighthill and Whitham in 1955 [32, 41]. The theory describes how traffic flow can become unstable and lead to the formation of waves of slowed or stopped traffic that propagate through the traffic stream. This theory laid the groundwork for kinematics-based traffic flow models, which describe how vehicles move in a traffic stream based on their kinematic properties.

Subsequent research has expanded upon these models, incorporating additional factors. The authors [13] delved into road surface irregularities, presenting a model that considers pothole depth, width, and critical density to discern their impact on traffic. Expanding the macroscopic perspective, [9] introduced a comprehensive model incorporating convection, anticipation, relaxation, diffusion, and viscosity, contributing to a holistic understanding of large-scale traffic dynamics. Khan's work brought forth a model analogous to Little's Law, establishing connections between traffic density, velocity, and time to enhance our comprehension of traffic behavior [27]. Another paper [50] addressed uncertainty in traffic velocity by formulating a continuum model that considers preceding vehicles on gradient highways, introducing parameters like gradient angle and uncertainty coefficient, also [47] delved into the electronic throttle dynamics on curved roads, incorporating variables such as slope angle and mass to capture the impact of electronic throttle control. In the same year [24] introduced a delayed-feedback control model based on throttle angle differences, aiming to enhance traffic stability through feedback mechanisms. The publication by [33] integrated time delay and anticipation effects into a macro traffic flow model, considering parameters like anticipation time and sensitivity coefficients, [43] brought stochastic elements into play with an advection diffusion equation, providing a realistic representation of random fluctuations in driver behavior, while [36] extended the Zhang model to include tailpipe emissions, shedding light on the environmental impact on traffic flow. In addition, [23] investigated a model encompassing diverse reactivity effects arising from driving attention and vehicle inertia, introducing sensitivity coefficients and other parameters.

Despite the development of these models, the macroscopic impact of the mean-field velocity difference on traffic flow models is still not well understood. This research seeks to explore the implications of this concept and its potential influence on a poor road network.

The following sections in the paper are organized as outlined below. The next section will explain how the model is derived, outlining the fundamental principles and assumptions. Following that, the third section will explore the stability of the model, using a linear approach to understand how the system behaves in different situations. Subsequently, we will closely examine non-linear traffic behaviors, such as the formation, and dissolution traffic waves. The final section will summarize the findings and draw meaningful conclusions that contribute to the progress of this field.

2. The Model

Understanding car-following behavior is crucial for analyzing traffic flow, predicting congestion, and developing strategies for traffic management and control. Some classical car-following models include [2, 14, 25]. Gazis et al. [14] introduced a groundbreaking car-following model that looks at how individual vehicles follow the lead of the car in front of them on a single-lane road, considering both their speed and the distance between them. Mathematically, this is expressed as:

$$v_n'(t+\Delta t) = \lambda \Delta v, \tag{2.1}$$

where $\Delta v = v_{n+1}(t) - v_n(t)$, representing the speed difference between the following and leading vehicles, with Δt as the reaction time and λ as a sensitivity coefficient.

However, the model had an unrealistic phenomenon where the leading and following vehicles were observed to be close to each other at identical speed levels. To correct this, Bando introduced the optimal velocity model [2], which considers the legal velocity of each car as a function of the distance headway with the model equation

$$v_n'(t) = \kappa \left[V(\Delta x_n(t)) - v_n(t) \right], \tag{2.2}$$

where $\kappa = 1/\tau$ represent the inverse of the driver's reaction time, $\Delta x = x_{n+1}(t) - x_n(t)$ represents the positional difference between two adjacent vehicles, and $V(\Delta x)$ is the optimal velocity of the following vehicle.

Despite its utility, experimental investigations revealed the OVM's issue of excessive acceleration and unrealistic deceleration. To overcome this issue, Helbing and Tilch [20] introduced a time lag of response into the OVM and modified the equation to include both positive and negative velocity differences. This led to the development of the full velocity difference model (FVDM), which takes into account the effects of both the gap headway between two vehicles and their respective speeds. The dynamic equation for the FVDM includes the optimal velocity and the velocity difference between the leading and following vehicles as:

$$v_n'(t) = \kappa \left[V(\Delta x_n(t)) - v_n(t) \right] + \lambda \Delta v_n(t). \tag{2.3}$$

Within the derivation process, the transformation of this micro model into a macro model is accomplished by employing the expansions outlined below.

$$v(x+\Delta, t) \equiv v(x,t) + v_x(x,t)\Delta, \tag{2.4}$$

$$\Delta v_n(t) \equiv v_{n+1}(t) - v_n(t) \equiv v(x+\Delta, t) - v(x,t) = \Delta v_x(x,t), \tag{2.5}$$

$$V(\Delta x_n(t)) \equiv V_e(k), \tag{2.6}$$

$$v_n'(t) \equiv v(x,t)v_x(x,t) + v_t(x,t), \tag{2.7}$$

where Δ is distance between two successive vehicles. Upon substituting equations (2.5, 2.6, 2.7) into equation (2.3), the resulting expression is:

$$v v_x + v_t = \frac{1}{\tau} \left[V_e(k) - v \right] + \lambda \Delta v_x. \tag{2.8}$$

In this paper, the adjustments made to the macro model (2.8) involve incorporating the mean-field velocity difference term $p(\Delta + l_o\theta)v_x$ [46] and the pothole effect ([13]) expressed as

$$\frac{1}{2}\pi\beta T \sqrt{\left(\frac{\beta^2}{4} + \alpha^2\right)} \left(1 - \frac{k}{k_{crit}}\right).$$

Consequently, the dynamic velocity equation is formulated as:

$$v v_x + v_t - p(\Delta + l_o\theta)]v_x = \frac{1}{\tau} \left[V_e(k) - v \right] + \lambda \Delta v_x - \frac{1}{2}\pi\beta T \sqrt{\left(\frac{\beta^2}{4} + \alpha^2\right)} \left(1 - \frac{k}{k_{crit}}\right). \tag{2.9}$$

The fundamental elements of the newly proposed model in this paper involve the integration of the dynamic density equation and the dynamic velocity equation as a system of partial differential equations

as

$$\begin{aligned} &k_t + (kv)_x = 0, \\ &v_t + [v - \lambda\Delta - p(\Delta + l_o\theta)]v_x = \frac{V_e - v}{\tau} - \frac{1}{2}\pi\beta T\sqrt{\left(\frac{\beta^2}{4} + \alpha^2\right)}\left(1 - \frac{k}{k_{crit}}\right), \end{aligned} \tag{2.10}$$

where $\theta \in (0,\ 1)$, p is the parameter of different mean-field velocity difference, l_o represents the length of a road in front of the current vehicle. α is the depth of the pothole and β is its width, k_{crit} denote the critical density, and T is the driver physiological reaction time. Together, these equations provide a comprehensive framework for understanding and modeling the dynamic behavior of a vehicular traffic flow.

3. Qualitative Properties of the Model

The second-order macroscopic model is composed of a continuity equation and a dynamic velocity equation. The proposed model is recast as:

$$\frac{\partial k}{\partial t} + v\frac{\partial k}{\partial x} + k\frac{\partial v}{\partial x} = 0, \tag{3.1}$$

$$\frac{\partial v}{\partial t} + (v - \lambda\Delta - p(\Delta + l_o\theta))\frac{\partial v}{\partial x} = \frac{V_e - v}{\tau} - \frac{1}{2}\pi\beta T\sqrt{\left(\frac{\beta^2}{4} + \alpha^2\right)}\left(1 - \frac{k}{k_{crit}}\right). \tag{3.2}$$

Equations (3.1) and (3.2) are cast into vectors and matrix to assess the qualitative characteristics:

$$\frac{\partial}{\partial t}\begin{bmatrix} k \\ v \end{bmatrix} + \begin{bmatrix} v & k \\ 0 & (v - \lambda\Delta - p(\Delta + l_o\theta)) \end{bmatrix}\frac{\partial}{\partial x}\begin{bmatrix} k \\ v \end{bmatrix} = \begin{bmatrix} 0 \\ \dfrac{V_e - v}{\tau} - \dfrac{1}{2}\pi\beta T\sqrt{(\dfrac{\beta^2}{4} + \alpha^2)}(1 - \dfrac{k}{k_{crit}}) \end{bmatrix}.$$

Let $\psi = [k, v]'$ and

$$C(\psi) = \begin{bmatrix} v & k \\ o & (v - \lambda\Delta - p(\Delta + l_o\theta)) \end{bmatrix},$$

$$D(\psi) = \begin{bmatrix} 0 \\ \dfrac{V_e - v}{\tau} - \dfrac{1}{2}\pi\beta T\sqrt{(\dfrac{\beta^2}{4} + \alpha^2)}(1 - \dfrac{k}{k_{crit}}) \end{bmatrix}.$$

We have

$$\frac{\partial \psi}{\partial t} + C(\psi)\frac{\partial \psi}{\partial x} = D(\psi). \tag{3.3}$$

When the source terms are set to zero, the derived homogeneous system can be represented in its quasi-linear form as:

$$\frac{\partial \psi}{\partial t} + C(\psi)\frac{\partial \psi}{\partial x} = 0. \tag{3.4}$$

The subsequent step involves determining the eigenvalues and eigenvectors. The Jacobian matrix is employed to ascertain the eigenvalues, given by:

$$|C - hI| = \begin{vmatrix} v - h & k \\ 0 & (v - \lambda\Delta - p(\Delta + l_o\theta)) - h \end{vmatrix} = 0.$$

This can be expanded as $(v-h)[(v-\lambda\Delta-p(\Delta+l_o\theta))-h] = 0$ which has two roots: $h_1 = v-\lambda\Delta-p(\Delta+l_o\theta)$ and $h_2 = v$ Thus, the eigenvalues representing the characteristic wave speed of the model are

$$\frac{dx_1}{dt} = v - \lambda\Delta - p(\Delta + l_o\theta) \ \text{ and } \ \frac{dx_1}{dt} = v.$$

It can be deduced that the model exhibits strict hyperbolicity. As a result, the traffic moves faster than the wave speed, and hence preserving the anisotropic nature of traffic flow. Now, the eigenvectors

are required to find the Riemann variables. The eigenvectors associated with the eigenvalue $(v - \lambda\Delta - p(\Delta + l_o\theta))$ is

$$\left[\frac{-k}{\lambda\Delta + p(\Delta + l_o\theta)},\ 1\right]'.$$

Similarly, the eigenvector relating to the other eigenvalue is $[1, 0]'$. Combining them give the matrix of eigenvectors W and its inverse W^{-1} as

$$W = \begin{bmatrix} \dfrac{-k}{\lambda\Delta + p(\Delta + l_o\theta)} & 1 \\ 1 & 0 \end{bmatrix} \text{ and } W^{-1} = \begin{bmatrix} 0 & 1 \\ 1 & \dfrac{k}{\lambda\Delta + p(\Delta + l_o\theta)} \end{bmatrix}.$$

A similarity matrix A is used to diagonalize the system, that is

$$C = WAW^{-1} \Longrightarrow A = W^{-1}CW.$$

Multiplying equation (3.3) by W^{-1} gives

$$W^{-1}\frac{\partial\psi}{\partial t} + W^{-1}C(\psi)\frac{\partial\psi}{\partial x} = W^{-1}D(\psi). \tag{3.5}$$

Presuming a minor alteration in $\delta\psi$, the derivative with respect to time is $\frac{\partial\psi}{\partial t}$, and the derivative with respect to the spatial variable is $\dfrac{\partial\psi}{\partial x}$. The modifications subsequently yield the Riemann variables as: $\delta z = W^{-1}\delta\psi$ and inversely as $\delta\psi = W\delta z$. Thus, $\partial z = W^{-1}\delta\psi$ can be expanded as:

$$\delta\begin{bmatrix} z_1 \\ z_2 \end{bmatrix} = \begin{bmatrix} 0 & 1 \\ 1 & \dfrac{k}{\lambda\Delta + p(\Delta + l_o\theta)} \end{bmatrix}\delta\begin{bmatrix} k \\ v \end{bmatrix}.$$

Expanding the above into separate equations will result in

$$\delta z_1 = \delta v \qquad \text{and} \qquad \delta z_2 = \delta k + \frac{k}{\lambda\Delta + p(\Delta + l_o\theta)}\delta v.$$

Upon integrating both sides, the wave propagation trajectories for this model are derived as

$$z_1 = v \text{ and } z_2 = k + \frac{k}{\lambda\Delta + p(\Delta + l_o\theta)}v.$$

Thus, the propagation of z_1 is along the characteristic $v(x, t)$, whereas the propagation of z_2 is along the characteristic $v(x, t) - (\lambda\Delta + p(\Delta + l_o\theta))$. This characteristic speed is associated with shock and rarefaction wave.

4. Linear Stability Analysis

Stop-and-go waves as well as phantom congestion indicate traffic instability. This segment pinpoints the specific parameter conditions that lead to a non-stationary flow. Assuming that k_e and v_e are the solutions to our proposed model, then a slight deviation from the steady state will be mathematically represented as:

$$k(x, t) = k_e + \delta k(x, t),$$
$$v(x, t) = v_e + \delta v(x, t).$$

Building upon the previous statement, we derive the fundamental linearized continuity equation as:

$$\frac{\partial(\delta k)}{\partial t} + v_e\frac{\partial(\delta k)}{\partial x} + k_e\frac{\partial(\delta v)}{\partial x} = 0. \tag{4.1}$$

Similarly, the linearized dynamic velocity equation is

$$\frac{\partial(\delta v)}{\partial t} + (v_e - \lambda\Delta - p(\Delta + l_o\theta))\frac{\partial(\delta v)}{\partial x} = \frac{1}{\tau}\left(\frac{dv}{dk}.\delta k - \delta v\right) - \frac{1}{2}\pi\beta T\sqrt{\left(\frac{\beta^2}{4} + \alpha^2\right)}\left(1 - \frac{k_e + \delta k}{k_{crit}}\right). \tag{4.2}$$

With the assumption that $k_e \sim k_{crit}$, equations (4.2) reduces to

$$\frac{\partial(\delta v)}{\partial t} + (v_e - \lambda\Delta - p(\Delta + l_o\theta))\frac{\partial(\delta v)}{\partial x} = \frac{1}{\tau}\left(\frac{dv}{dk}.\delta k - \delta v\right) + \frac{1}{2}\pi\beta T\sqrt{\left(\frac{\beta^2}{4} + \alpha^2\right)}\left(\frac{\delta k}{k_{crit}}\right). \tag{4.3}$$

We assume that the disturbance $\delta k(x,t), \delta v(x,t)$ can be mimicked using the simple wave equation.

$$\delta k(x,t) = k_* \exp[isx + (\lambda - i\omega)t] = k_* e^{\lambda t} e^{i(sx-\omega t)}, \tag{4.4a}$$

$$\delta v(x,t) = v_* \exp[isx + (\lambda - i\omega)t] = v_* e^{\lambda t} e^{i(sx-\omega t)}. \tag{4.4b}$$

where s and ω are the wave number and speed respectively, and growth rate Λ. Slight changes in Λ could lead to phantom traffic jam when $\Lambda > 0$.

Substituting (4.4) and its derivatives into the continuity equation

$$(\Lambda - i\omega)k_* e^{\Lambda t} e^{i(sx-\omega t)} + v_e i s k_* e^{\Lambda t} e^{\Lambda t} e^{i(sx-\omega t)} + k_e i s v_* e^{\Lambda t} e^{i(sx-\omega t)} = 0$$

and the momentum equation

$$\begin{aligned}&(\Lambda - i\omega)v_* e^{\Lambda t} e^{i(sx-\omega t)} + (v_e - \lambda\Delta - p(\Delta + l_o\theta))isv_* e^{\Lambda t} e^{\Lambda t} e^{i(sx-\omega t)}\\ &= \frac{1}{\tau}\left(\frac{dv}{dk}.k_* e^{\Lambda t} e^{\Lambda t} e^{i(sx-\omega t)} - v_* e^{\Lambda t} e^{\Lambda t} e^{i(sx-\omega t)}\right) + \frac{1}{2}\pi\beta T\sqrt{\left(\frac{\beta^2}{4} + \alpha^2\right)}\left(\frac{k_* e^{\Lambda t} e^{\Lambda t} e^{i(sx-\omega t)}}{k_{crit}}\right).\end{aligned} \tag{4.5}$$

The linearized continuity and dynamic velocity equation are rearranged as

$$e^{\Lambda t} e^{i(sx-\omega t)}(k_*(\Lambda - i\omega) + v_e i s k_* + k_e i s v_*) = 0, \tag{4.6}$$

$$\begin{aligned}&e^{\Lambda t} e^{i(sx-\omega t)}\left[v_*(\Lambda - i\omega) + (v_e - \lambda\Delta - p(\Delta + l_o\theta))isv_* - \frac{1}{\tau}\left(\frac{dv}{dk}.k_* - v_*\right)\right.\\ &\left. - \frac{1}{2}\pi\beta T\sqrt{\left(\frac{\beta^2}{4} + \alpha^2\right)}\left(\frac{k_*}{k_{crit}}\right)\right] = 0.\end{aligned} \tag{4.7}$$

Equations (4.6) and (4.7) are simplified using matrix notation as

$$\begin{bmatrix} \Lambda - i\omega + v_e i s & k_e i s \\ -\dfrac{dv}{\tau dk} - \dfrac{V}{k_{crit}} & (\Lambda - i\omega) + (v_e - \lambda\Delta - p(\Delta + l_o\theta))is + \dfrac{1}{\tau} \end{bmatrix} \begin{bmatrix} k_* \\ v_* \end{bmatrix} = \begin{bmatrix} 0 \\ 0 \end{bmatrix}$$

where

$$V = \frac{1}{2}\pi\beta T\sqrt{\left(\frac{\beta^2}{4} + \alpha^2\right)}.$$

Letting $\overline{\Lambda} = \Lambda - i\overline{\omega}$ and $\overline{\omega} = \omega - v_e s$, the above matrix equation is rewritten as

$$\begin{bmatrix} \overline{\Lambda} & k_e i s \\ -\dfrac{dv}{\tau dk} - \dfrac{V}{k_{crit}} & \overline{\Lambda} - (\lambda\Delta + p(\Delta + l_o\theta))is + \dfrac{1}{\tau} \end{bmatrix} \begin{bmatrix} k_* \\ v_* \end{bmatrix} = \begin{bmatrix} 0 \\ 0 \end{bmatrix}.$$

From the homogeneous part, the characteristic equation is:

$$\overline{\Lambda^2} + \overline{\Lambda}\left(\frac{1}{\tau} - (\lambda\Delta + p(\Delta + l_o\theta))is\right) + k_e i s\left(\frac{dv}{\tau dk} + \frac{V}{k_{crit}}\right) = 0.$$

But

$$\Lambda_{1,2} = -\frac{b}{2} \pm \sqrt{\left(\frac{b}{2}\right)^2 - c}\,.$$

The solution to the characteristic polynomial is obtained as:

$$\overline{\Lambda_{1,2}} = \frac{1}{2}\left((\lambda\Delta + p(\Delta + l_o\theta))is - \frac{1}{\tau}\right) \pm \sqrt{\frac{1}{4}\left(- ((\lambda\Delta + p(\Delta + l_o\theta))is + \frac{1}{\tau}\right)^2 - k_e is\left(\frac{dv}{\tau dk} + \frac{V}{k_{crit}}\right)}$$

which can be expanded as

$$\overline{\Lambda_{1,2}} = \frac{1}{2}\left((\lambda\Delta + p(\Delta + l_o\theta))is\right) - \frac{1}{2\tau} \pm \sqrt{\frac{1}{4\tau^2} - \frac{(\lambda\Delta + p(\Delta + l_o\theta))^2 s^2}{4} - \left(k_e s\left(\frac{dv}{\tau dk} + \frac{V}{k_{crit}}\right) + \frac{(\lambda\Delta + M\Delta)s}{2}\right)i},$$

which can be further expressed as

$$\overline{\Lambda_{1,2}} = \frac{1}{2}\left((\lambda\Delta + p(\Delta + l_o\theta))is\right) - \frac{1}{2\tau} \pm \sqrt{R + i|I|},$$

where

$$R = \frac{1}{4\tau^2} - \frac{(\lambda\Delta + p(\Delta + l_o\theta))^2 s^2}{4}$$

and

$$|I| = -\left[k_e s\left(\frac{1}{\tau}\frac{dv}{dk} + \frac{V}{k_c rit}\right) + \frac{(\lambda\Delta + p(\Delta + l_o\theta)s}{2\tau}\right].$$

Following from [19, 22]

$$\sqrt{R + i|I|} = \left[\frac{1}{2}(\sqrt{R^2 + I^2} + R)\right]^{\frac{1}{2}} + i\left[\frac{1}{2}(\sqrt{R^2 + I^2} - R)\right]^{\frac{1}{2}}.$$

Hence,

$$\overline{\Lambda_{1,2}} = \frac{1}{2}\left((\lambda\Delta + p(\Delta + l_o\theta))is\right) - \frac{1}{2\tau} \pm \left[\left[\frac{1}{2}(\sqrt{R^2 + I^2} + R)\right]^{\frac{1}{2}} + i\left[\frac{1}{2}(\sqrt{R^2 + I^2} - R)\right]^{\frac{1}{2}}\right]. \quad (4.8)$$

Equation (4.8) can be separated into real and imaginary part as

$$R\varepsilon(\overline{\Lambda_{1,2}}) = -\frac{1}{2\tau} \pm \left[\frac{1}{2}(\sqrt{R^2 + I^2} + R)\right]^{\frac{1}{2}}$$

and

$$IM(\overline{\Lambda_{1,2}}) = \frac{1}{2}\left[(\lambda\Delta + p(\Delta + l_o\theta))is\right] \pm i\left[\frac{1}{2}(\sqrt{R^2 + I^2} - R)\right]^{\frac{1}{2}}.$$

This implies that

$$R\varepsilon(\overline{\lambda_1}) = -\frac{1}{2\tau} + \left[\frac{1}{2}(\sqrt{R^2 + I^2} + R)\right]^{\frac{1}{2}},$$

$$R\varepsilon(\overline{\lambda_2}) = -\frac{1}{2\tau} - \left[\frac{1}{2}(\sqrt{R^2 + I^2} + R)\right]^{\frac{1}{2}}.$$

Considering the criteria mentioned earlier, it suggests that if $R\varepsilon(\Lambda_1)$ is more than zero, $R\varepsilon(\Lambda_2)$ will also be greater than zero. This is because $R\varepsilon(\Lambda_1)$ exceeds $R\varepsilon(\Lambda_2)$. For $R\varepsilon(\Lambda_2)$, the same instability condition that holds for $R\varepsilon(\Lambda_1)$ will apply. The stability of the new model will be attained, when $R\varepsilon(\Lambda_1)$ is smaller than zero, that is, when

$$-\frac{1}{2\tau} + \left[\frac{1}{2}(\sqrt{R^2 + I^2} + R)\right]^{\frac{1}{2}} \leq 0,$$

which can be simplified as

$$I^2 \leq \frac{1}{4\tau^4} - \frac{R}{\tau^2}. \tag{4.9}$$

From the previous analysis, we realize that

$$R = \frac{1}{4\tau^2} - \frac{(\lambda\Delta + p(\Delta + l_o\theta))^2 s^2}{4}$$

and

$$I = -\left[k_e s\left(\frac{1}{\tau}\left|\frac{dv}{dk}\right| + \frac{V}{k_{crit}}\right) + \frac{(\lambda\Delta + p(\Delta + l_o\theta))s}{2\tau}\right].$$

These real and imaginary terms are substituted into Equation (4.9). That is:

$$\left[-k_e s\left(\frac{1}{\tau}\left|\frac{dv}{dk}\right| + \frac{V}{k_{crit}}\right) - \frac{(\lambda\Delta + p(\Delta + l_o\theta))s}{2\tau}\right]^2 \leq \frac{1}{4\tau^4} - \frac{1}{\tau^2}\left[\frac{1}{4\tau^2} - \frac{(\lambda\Delta + p(\Delta + l_o\theta))^2 s^2}{4}\right].$$

Expanding and simplifying

$$\left[k_e s\left(\frac{1}{\tau}\left|\frac{dv}{dk}\right| + \frac{V}{k_{crit}}\right)\right] \times \left[k_e s\left(\frac{1}{\tau}\left|\frac{dv}{dk}\right| + \frac{V}{k_{crit}}\right) + \frac{(\lambda\Delta + p(\Delta + l_o\theta))s}{\tau}\right] \leq 0,$$

implying that

$$k_e s\left(\frac{1}{\tau}\left|\frac{dv}{dk}\right| + \frac{V}{k_{crit}}\right) + \frac{(\lambda\Delta + p(\Delta + l_o\theta))s}{\tau} \leq 0.$$

Thus the stability condition is

$$k_e\left(\left|\frac{dv}{dk}\right| + \frac{V\tau}{k_{crit}}\right) + (\lambda\Delta + p(\Delta + l_o\theta)) \leq 0. \tag{4.10}$$

The stability condition derived from the model offers a comprehensive framework for analyzing and improving traffic flow stability. The model's stability relies on some major parameters, and it is essential to recognize and oversee these factors to avoid major disruptions.

5. Numerical Simulation

In this section, we will be exploring how density and velocity varies across the space and time domain for macroscopic flow. Our investigation will involve the use of numerical simulations to examine the impact of minor disturbances.

Prior to implementing the numerical approach, we convert the continuous differential equation presented in (3.1) and (3.2) into a discretized version in the following manner:

$$k_i^{j+1} = \frac{\Delta t}{\Delta x} k_i^j (v_i^j - v_{i+1}^j) + \frac{\Delta t}{\Delta x} v_i^j (k_{i-1}^j - k_i^j). \tag{5.1}$$

Heavy traffic (i.e $v_i^j < c_c$):

$$v_i^{j+1} = v_i^j - \frac{\Delta t}{\Delta x}(v_i^j - c_c)(v_{i+1}^j - v_i^j) + \frac{\Delta t(v_e(k_i^j) - v_i^j)}{\tau} - \frac{1}{2}\Delta t\pi\beta T\sqrt{\left(\frac{\beta^2}{4} + \alpha^2\right)\left(1 - \frac{k_i^j}{k_{crit}}\right)}. \tag{5.2}$$

Smooth traffic (i.e $v_i^j > c_c$):

$$v_i^{j+1} = v_i^j - \frac{\Delta t}{\Delta x}(v_i^j - c_c)(v_i^j - v_{i-1}^j) + \frac{\Delta t(v_e(k_i^j) - v_i^j)}{\tau} - \frac{1}{2}\Delta t\pi\beta T\sqrt{\left(\frac{\beta^2}{4} + \alpha^2\right)\left(1 - \frac{k_i^j}{k_{crit}}\right)}. \tag{5.3}$$

where $c_c = \lambda\Delta + p(\Delta + l_o\theta)$, k_i^j and v_i^j are respectively the density and velocity information on the condition (i, j), i and j represent the space section and time interval; Δx and Δt respectively represent spatial steps and time step.

5.1. **Shock waves and rarefaction waves.** We will conduct a simulation tests to assess the ability of our newly proposed macro model to accurately represent shock waves and rarefaction waves. This will allow us to evaluate the effectiveness of the model and determine its capabilities in accurately depicting traffic flow under varying conditions.

Outlined below are the characteristics of the two Riemann initial conditions

$$k_{up}^1 = 0.019(veh/m), \qquad k_{down}^1 = 0.910(veh/m),$$
$$k_{up}^2 = 0.910(veh/m), \qquad k_{down}^2 = 0.019(veh/m),$$

where k_{up} and k_{down} are respectively the upstream and downnstream densities of shock and rarefaction waves.

The initial speed profiles can be expressed as follows:

$$v_{up}^{1,2} = v_e(k_{up}^{1,2}),$$
$$v_{down}^{1,2} = v_e(k_{down}^{1,2}).$$

We again consider the following speed-density equation [7, 10]

$$V_e = v_f \left[1 - \exp\left(1 - \exp\left(\frac{c_m}{v_f}\left(\frac{k_m}{k} - 1\right)\right)\right)\right], \tag{5.4}$$

where v_f represents the free flow velocity; k_m is the maximum density; c_m is for the kinematic wave velocity. The road length L of 1000 meters, divided into 100 grids, with time step of 0.1 seconds, and the remaining parameters are specified in Table 1. These are benchmark data values widely accepted in the literature and are based on real traffic experiments. They have been used extensively in the study of traffic flow dynamics and have been instrumental in the development and validation of various traffic models and simulation techniques.

Table 1. Parameter Setup

Parameter	Value
v_f	25.00 m/s
k_m	1.00 veh/m
c_m	9.00 m/s
λ	0.60
θ	0.50
p	1.00 m/s
l_0	4.00 m
τ	3.00
α	[0.10 0.30]m
β	[0.04 2.4]m
Δ	4. 00m
T	1.00 s
k_{crit}	0.38 veh/m

From Figure 1, the velocity profiles for roads with small and large size potholes provide a stark contrast in traffic flow behavior. Small size potholes, assumed to have a conical form with a depth of 0.1 meters and a width of 0.4 meters, allow vehicles on the corresponding road to reach their maximum speed prior to encountering the shockwave. This results in a relatively smooth traffic flow, with a small

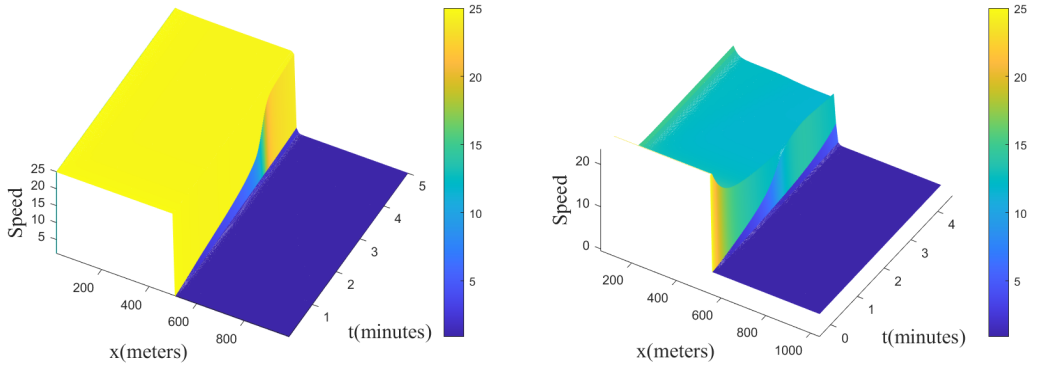

FIGURE 1. Shock waves for the evolution of velocity for road with small size potholes (left), and large size potholes (right)

buildup of cars upstream of the shock. However, this buildup quickly dissipates due to the limited number of vehicles catching up with the shock.

In contrast, large size potholes, with a depth of 0.3 meters and a width of 2.4 meters, create significant challenges for drivers. Vehicles on the road with large potholes struggle to reach their maximum speed, even when the road ahead is clear. This leads to a gradual decline in speed towards the region of dense vehicles downstream of the shock. Consequently, there is a more substantial buildup of cars upstream of the shock compared to the road with small potholes.

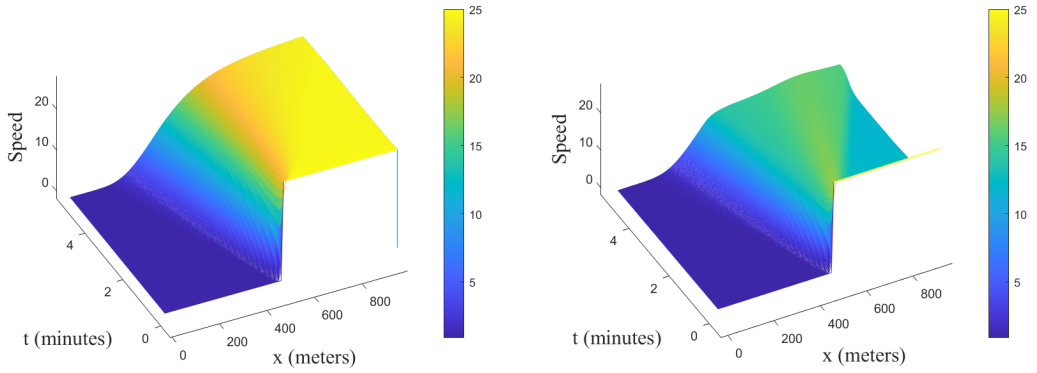

FIGURE 2. Rarefaction waves for the evolution of velocity for road with small size potholes (left), and large size potholes (right)

The rarefaction plots in Figure 2 presents a notable comparison between traffic flow on roads with small and large size potholes. On the road with small potholes, vehicles can efficiently achieve their maximum speed as the queue dissolves, resulting in smooth traffic flow. Despite heavy traffic upstream, drivers maintain a relatively low speed rate. Moreover, due to the light density downstream, vehicles quickly reach their maximum velocity, indicating efficient traffic dissipation.

In contrast, the road with large potholes shows a different pattern. Despite an empty road ahead after the dissolution of the queue, vehicles on this road struggle to reach their maximum speed. The velocity profile reflects a persistent low-speed rate, highlighting the challenges posed by the road condition.

This contrasts sharply with the behavior observed on the road with small potholes, where drivers can efficiently reach their maximum speeds. Despite the absence of congestion downstream, vehicles on the road with large potholes are unable to attain their maximum velocities efficiently.

These observations provide valuable insights into the impact of pothole size on traffic flow dynamics. The impact on congestion is evident, with roads containing large potholes experiencing increased traffic buildup and reduced speeds. The dissipation of traffic buildup upstream of the shock is slower on roads with large potholes, highlighting the challenges faced by drivers in such conditions. The rarefaction wave profiles also align with real-world scenarios, emphasize the critical role of road maintenance. Roads with small potholes allow for efficient traffic dissipation and quick attainment of maximum velocity, leading to smoother traffic flow. Conversely, roads with large potholes present persistent challenges for drivers, indicating the need for timely maintenance to ensure improved traffic flow and better driving experiences.

6. Local Cluster Effect

The local cluster effect refers to the stop-and-go patterns observed in traffic flow due to minor disruptions. This section delves into the examination of the local cluster effect in the context of a localized disturbance under a constant, uniform condition. In this research, we utilize the average density k_0 as suggested by [21]:

$$k(x,0) = k_0 + \Delta k_0 \left\{ \cosh^{-2}\left[\frac{160}{L}\left(x - \frac{5L}{16}\right)\right] - \frac{1}{4}\cosh^{-2}\left[\frac{40}{L}\left(x - \frac{11L}{32}\right)\right]\right\},$$

where L is the road length, k_0 represents the initial constant density, and $\Delta k_0 = 0.2veh/m$ signifies the amplitude of a localized disturbance. The initial density k_0 will be retained as a free parameter to quantify the extent of cluster effects. The periodic boundary conditions are adopted, there exist $k(L,t) = k(0,t)$ and $v(L,t) = v(0,t)$.

Here, we adapt the following speed-density equation [10]:

$$V_e(k) = v_f \left[\left(1 + \exp\frac{k/k_m - 0.25}{0.06}\right)^{-1} - 3.72 \times 10^{-6}\right],$$

where k_m denotes the maximum density.

Figures 3 and 4 highlights the impact of small changes in the initial density profile of the traffic stream. Snapshots of the simulation demonstrate that when the initial traffic density ranges between 0.2 veh/m and 0.35 veh/m, the density experiences significant fluctuations. Four initial density profiles are considered.

As the initial density increases, the disturbance in the wave profiles also intensifies. The traffic flow evolves into multiple local clusters, leading to the stop-and-go phenomenon. Beyond a certain point, the effect of the disturbance becomes insignificant, resulting in a more uniform flow. This observation indicates that small changes in the initial density can have a substantial impact on the traffic flow dynamics.

When comparing the profiles for roads with small size potholes (Figure 3) and roads with large size potholes (Figure 4), the effect of changes in the initial density is more pronounced for the road in good condition. The snapshots reveal that the road with small potholes is more sensitive to variations in initial density, showing clearer fluctuations and cluster formations. Conversely, the road with large potholes exhibits less sensitivity to changes in initial density, indicating a more stable traffic flow pattern despite variations in the starting density. This comparison present the influence of road condition on how traffic flow responds to changes in initial conditions, with the road quality playing a significant role in the formation and dissipation of traffic clusters.

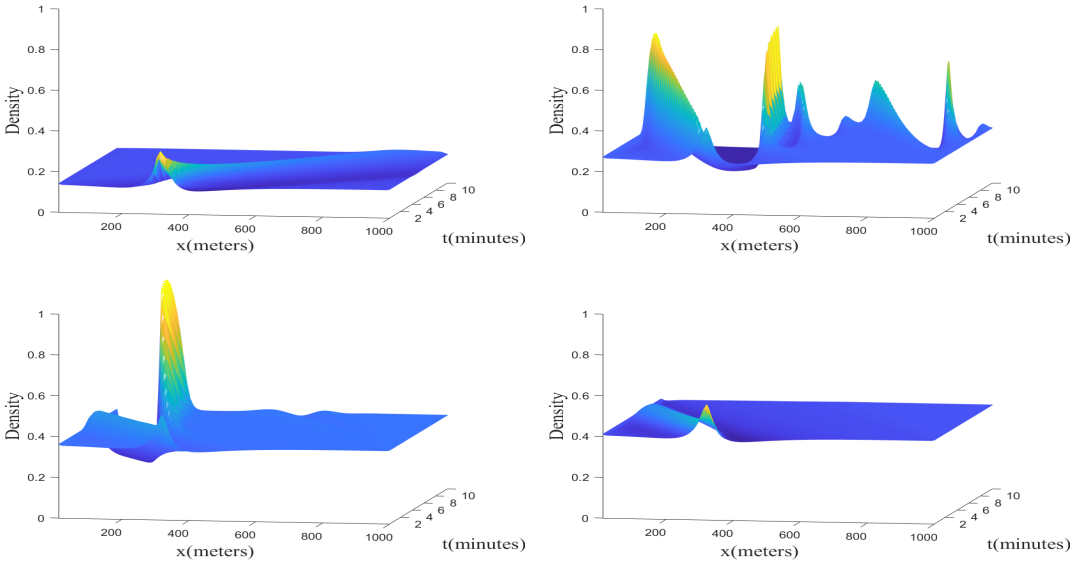

FIGURE 3. Space–time evolution of small perturbation for road with small size potholes. The initial density profiles are given as $k_0 = 0.14$(top left), $k_o = 0.27$(top right), $k_o = 0.36$(bottom left), $k_o = 0.41$(bottom right)

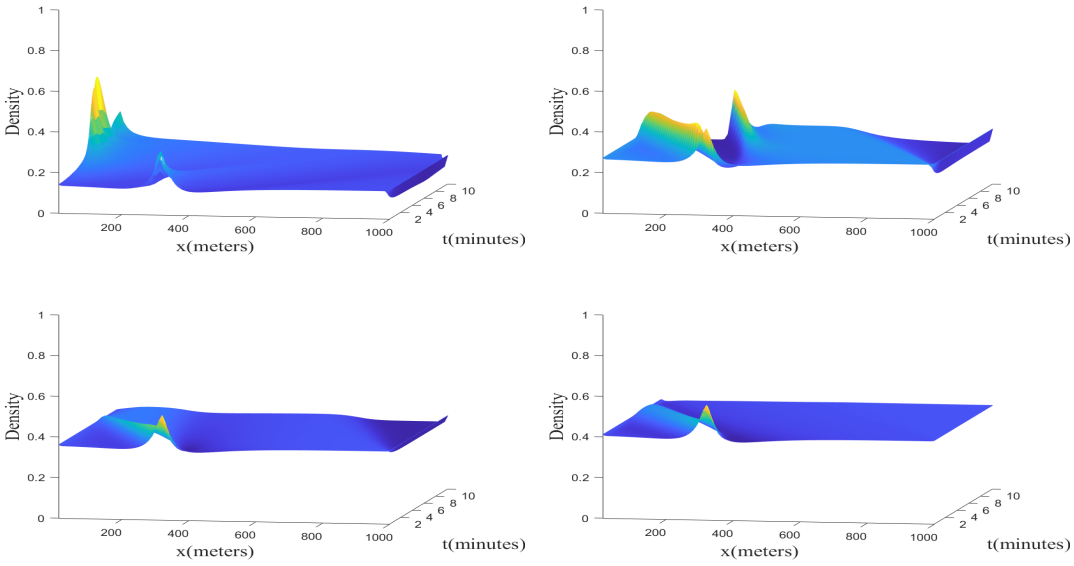

FIGURE 4. Space–time evolution of small perturbation for road with large size potholes. The initial density profiles are given as $k_0 = 0.14$(top left), $k_o = 0.27$(top right), $k_o = 0.36$(bottom left), $k_o = 0.41$(bottom right)

In exploring the impact of the mean-field velocity difference p on traffic flow, we perturbed the system to observe the maximum cluster effect. Four scenarios were examined with varying p values as presented in Figures 5 and 6.

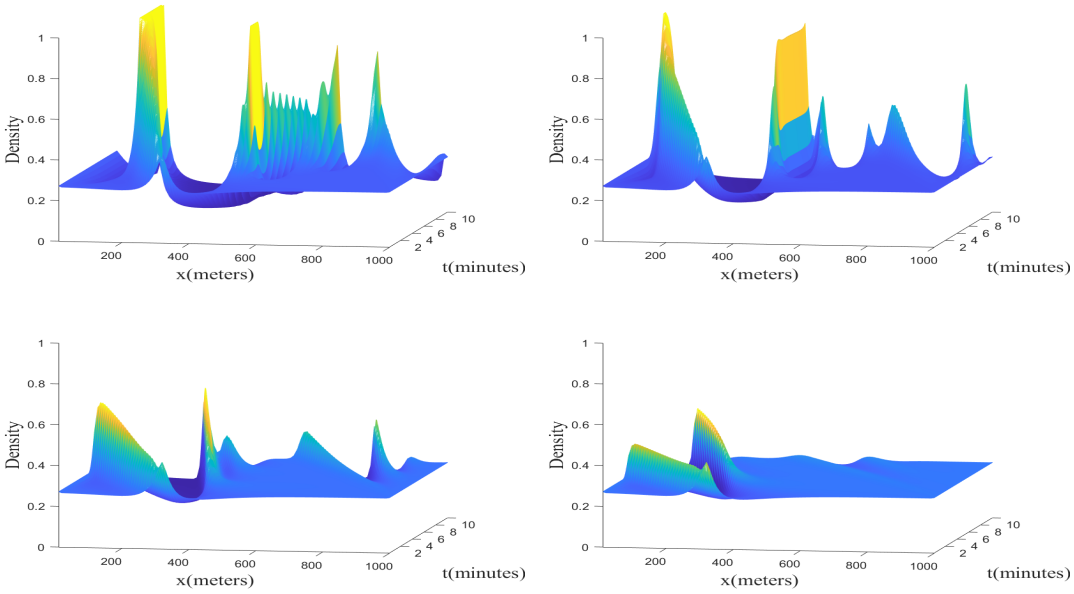

FIGURE 5. Space–time evolution for small sized potholed road with $k_o = 0.27$, and $p = 0.00$(top left), $p = 0.70$(top top right), $p = 1.40$(bottom left), $p = 2.00$(bottom right)

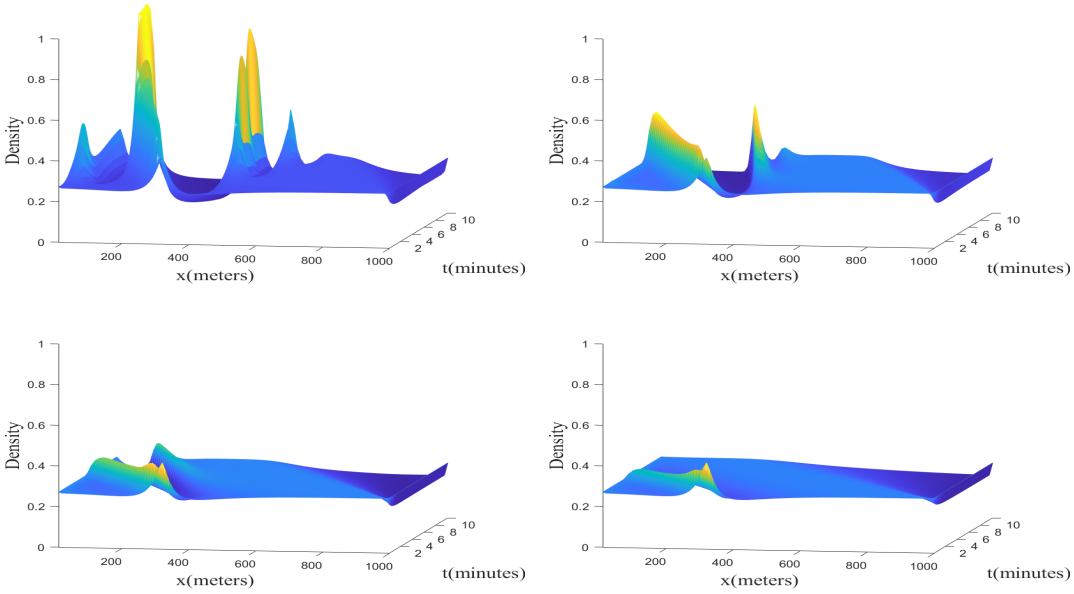

FIGURE 6. Space–time evolution for large sized potholed road with $k_o = 0.27$, and $p = 0.00$(top left), $p = 0.70$(top top right), $p = 1.40$(bottom left), $p = 2.00$(bottom right)

It was observed that the amplitudes of the density profile for these clusters increase significantly as the mean-field velocity difference approaches zero. This phenomenon indicates that when p is closer to zero, the traffic flow experiences more pronounced clustering behavior, leading to the stop-and-go

pattern. This result aligns with our understanding of how small perturbations in p can cause substantial changes in traffic dynamics.

Moreover, the effect of these perturbations is more pronounced on the road in good condition (Figure 5) compared to the road with bad potholes (Figure 6). The snapshots of the simulation clearly illustrate that the road with small potholes is more sensitive to variations in p, exhibiting larger and more defined clusters as p approaches zero. On the other hand, the road with large potholes shows less sensitivity to changes in p, maintaining a relatively uniform flow pattern despite variations in the mean-field velocity difference.

These results emphasize the significant influence of p on the formation of traffic clusters, particularly on roads with different pothole sizes. The road quality plays a crucial role in how traffic responds to changes in p, with roads in better condition showing greater sensitivity to variations in the mean-field velocity difference. This insight provides valuable information for understanding how road conditions and mean-field velocity differences interact to affect traffic flow patterns and the occurrence of congestion.

7. Conclusion

This paper introduces a comprehensive macroscopic traffic flow model that incorporates the mean-field velocity difference in the context of adverse road conditions. The study addresses the challenges of traffic congestion, especially in the presence of poor road networks. The proposed model builds upon foundational traffic flow theories and integrates elements such as pothole effects, mean-field velocity difference into the dynamic velocity equations. The theoretical framework of the derived model is supported by a linear stability analysis, providing insights into the stability conditions crucial for effective traffic control.

The numerical simulations demonstrate the model's ability to accurately depict shock waves, rarefaction waves, and the local cluster effect under various conditions. Notably, the model proves successful in imitating the abrupt impact of shock waves and the dissolution of rarefaction waves, with apparent variation for fairly good and bad roads. The investigation revealed that roads with small potholes allow vehicles to achieve maximum speed prior to encountering shocks, resulting in smoother traffic flow. In contrast, roads with large potholes present challenges for drivers, who struggle to reach maximum speed even on clear stretches of road. This disparity is further highlighted by the pronounced effect of small changes in initial traffic density, particularly on roads in better condition.

The numerical experiments further highlight the model's adaptability to dynamic density changes and its success in mimic the local cluster effect. Moreover, the study uncovered a cluster effect, where small perturbations in the mean-field velocity difference led to significant fluctuations in traffic density. As the mean-field velocity difference approached zero, the amplitude of density profiles increased, resulting in the formation of traffic clusters and the stop-and-go phenomenon. This effect was more pronounced on roads with small potholes, showcasing the sensitivity of road conditions to changes in traffic flow dynamics.

The proposed model's unique contribution lies in its consideration of mean-field velocity differences on a poor road network, addressing a gap in existing macroscopic traffic flow models. This research opens avenues for further exploration and refinement of traffic flow models, fostering a deeper understanding of complex traffic dynamics and informing strategies for efficient traffic management in adverse conditions.

References

[1] W. H. Ai, M. M. Wang, and D. W. Liu, *Analysis of macroscopic traffic flow model considering throttle dynamics*, Eur. Phys. J. B **96**(2023): 87.

[2] M. Bando, K. Hasebe, A. Nakayama, A. Shibata, and Y. Sugiyama, *Dynamical model of traffic congestion and numerical simulation*, Phys. Rev. E **51**(1995): 1035.
[3] S. C. Benjamin, N. F. Johnson, and P. Hui, *Cellular automata models of traffic flow along a highway containing a junction*, J. Phys. A: Math. Gen. **29**(1996), 3119–3127.
[4] S. Bexelius, *An extended model for car-following*, Transp. Res. **2**(1968), 13–21.
[5] R. Chandler, R. Herman, and E. Montroll, *Traffic dynamics: Studies in car following*, Oper. Res. **6**(1958), 165–184.
[6] C. F. Daganzo, *The cell transmission model: A dynamic representation of highway traffic consistent with the hydrodynamic theory*, Transp. Res. Part B: Methodol. **28**(1994), 269–287.
[7] J. M. Del Castillo and F. G. Benitez, *On functional form of the speed-density relationship - i: general theory, ii: empirical investigation*, Transp. Res. B **29**(1995), 373–406.
[8] L. C. Eddie, *Car-following and steady-state theory for noncongested traffic*, Oper. Res. **9**(1961), 66–76.
[9] G. O. Fosu, A. Adu-Sackey, and J. Ackora-Prah, *Macroscopic analysis of the viscous-diffusive traffic flow model*, Math. Appl. Sci. Eng. (2022), 1–12.
[10] G. O. Fosu, E. Akweittey, J. M. Opong, and M. E. Otoo, *Vehicular traffic models for speed-density-flow relationship*, J. Math. Model. **8**(2020), 241–255.
[11] G. O. Fosu and F. T. Oduro, *Two dimensional anisotropic macroscopic second-order traffic flow model*, J. Appl. Math. Comput. Mech. **19**(2020), 59-71.
[12] G. O. Fosu, F. T. Oduro, and C. Caligaris, *Multilane analysis of a viscous second-order macroscopic traffic flow model*, SN Part. Diff. Equ. Appl. **2**(2021), 1–17.
[13] G. O. Fosu, J. M. Opong, B. E. Owusu, and S. M. Naandam, *Modeling road surface potholes within the macroscopic flow framework*, Math. Appl. Sci. Eng. **3**(2022), 106–118.
[14] D. C. Gazis, R. Herman, and R. W. Rothery, *Nonlinear follow-the-leader models of traffic flow*, Oper. Res. **9**(1961), 545–567.
[15] H.-X. Ge, Y. Cui, K.-Q. Zhu, and R.-J. Cheng, *The control method for the lattice hydrodynamic model*, Commun. Nonlinear Sci. Numer. Simul. **22**(2015), 903–908.
[16] H. H. Gidey and S. M. Kassa, *Extended second-order multiclass traffic flow model with the relative drag function*, Available at SSRN 4374659 (2023).
[17] S. Gobron and N. Chiba, *Crack pattern simulation based on 3D surface cellular automaton*, The Visual Comput. - Special Issue: Comput. Graph. Int. **17**(2001), 287–309.
[18] J. Greenberg, A. Klar, and M. Rascle, *Congestion on multilane highways*, SIAM J. Appl. Math. **63**(2003), 818–833.
[19] D. Helbing and A. F. Johansson, *On the controversy around Daganzo's requiem for and Aw-Rascle's resurrection of second-order traffic flow models*, Eur. Phys. J. B **69** (2009), 549–562.
[20] D. Helbing and M. Schreckenberg, *Cellular automata simulating experimental properties of traffic flow*, Phys. Rev. E Stat. Nonlin. Soft Matter Phys. **59**(1999), R2505-R2508.
[21] M. Herrmann and B. S. Kerner, *Local cluster effect in different traffic flow models*, Physica A **255**(1998), 163–188.
[22] S. P. Hoogendoorn, *Traffic flow theory and simulation*, Transp. Traffic Eng. Sect. Faculty Civ. Eng. Geosciences, Delft Univ. Technol. (2005).
[23] M. A. Hossain and T. Jun, *Diverse reactivity model for traffic flow dynamics in Eulerian scope*, Nonlinear Dyn. **111**(2023), 17369-17378.
[24] A. Jafaripournimchahi, Y. Cai, H. Wang, L. Sun, and B. Yang, *Stability analysis of delayed-feedback control effect in the continuum traffic flow of autonomous vehicles without V2I communication*, Physica A Stat. Mech. Appl. **605**(2022): 127975.
[25] R. Jiang, Q. Wu, and Z. Zhu, *Full velocity difference model for a car-following theory*, Phys. Rev. E **64**(2001): 017101.
[26] B. S. Kerner, S. L. Klenov, and D. E. Wolf, *Cellular automata approach to three phase traffic theory*, J. Phys. A Math. Gen. **35**(2002): 9971.
[27] Z. H. Khan, T. A. Gulliver, W. Imran, K. S. Khattak, A. B. Altamimi, and A. Qazi, *A macroscopic traffic model based on relaxation time*, Alex. Eng. J. **61**(2022), 585–596.
[28] L. Leclercq and J. A. Laval, *A multiclass car-following rule based on the LWR model, in: Appert-Rolland, C., F. Chevoir, P. Gondret, S. Lassarre, J.-P. Lebacque, M. Schreckenberg, eds.*, in *Traffic and Granular Flow*, Springer, Berlin Heidelberg, 2007.
[29] H. Lenz, C. K. Wagner, and R. Sollacher, *Multi-anticipative car-following model*, Eur. Phys. J. B Condens. Matter Complex Syst. **7**(1999), 331–335.
[30] C.-Y. Li, T.-Q. Tang, H.-J. Huang, and H.-Y. Shang, *A new car-following model with consideration of driving resistance*, Chin. Phys. Lett. **28**(2011): 038902.

[31] X.-G. Li, B. Jia, Z.-Y. Gao, and R. Jiang, *A realistic two-lane cellular automata traffic model considering aggressive lane-changing behavior of fast vehicle*, Physica A Stat. Mech. Appl. **367** (2006), 479–486.
[32] M. J. Lighthill and G. B. Whitham, *On kinematic waves II: A theory of traffic flow on long crowded roads*, Proc. Roy. Soc. Lond. A Math. Phys. Sci. **229**(1955), 317–345.
[33] H. Lyu, R. Cheng, and H. Ge, *Bifurcation analysis of an extended macro model considering time delay and anticipation effect*, Physica A Stat. Mech. Appl. **585**(2022): 126434.
[34] G. F. Newell, *Nonlinear effects in the dynamics of car following*, Oper. Res. **9**(1961), 209-229.
[35] L. A. Pipes, *Car following models and the fundamental diagram of road traffic*, Transp. Res. **1**(1967), 21–29.
[36] T. Qaiser and F. A. Khan, *Macroscopic traffic flow model based on vehicular emissions*, Int. Res. J. Modernization Eng. Technol. Sci. **4**(2022), 1800–1805.
[37] W. Qi, H. Wen, Y. Wu, and L. Qin, *Effect model of urban traffic congestion on driver's lane-changing behavior*, SAGE Adv. Mech. Eng. **9**(2017), 1–12.
[38] D. Qiao, B. Dai, Z. Lin, M. Guo, X. Zhang, P. Zhang, and F. Cheng, *Study on vehicle fuel consumption and exhaust emissions based on a new viscous macroscopic traffic flow model*, J. Transp. Eng. Part A Syst. **149**(2023): 04022137.
[39] F. Rajé, M. Tight, and F. D. Pope, *Traffic pollution: A search for solutions for a city like Nairobi*, Cities **82**(2018), 100–107.
[40] P. Redhu and A. K. Gupta, *Delayed-feedback control in a lattice hydrodynamic model*, Commun. Nonlinear Sci. Numer. Simul. **27**(2015), 263–270.
[41] P. I. Richards, *Shock waves on the highway*, Oper. Res. **4**(1956), 42–51.
[42] P. R. Stopher, *Reducing road congestion: a reality check*, Transp. Policy **11** (2004), 117–131.
[43] J. P. Wakefield and S. Karni, *Traffic flow models with noise*, in: XVIII International Conference on Hyperbolic Problems: Theory, Numer. Appl., Málaga, June 20-24, pp.467–476.
[44] T. Wang, *A new macro model for traffic flow considering the driver's delay effect*, in *2013 25th Chinese Control and Decision Conference (CCDC)*, IEEE (2013), 4535–4537.
[45] Y.-Q. Wang, C.-F. Zhou, B.-W. Yan, D.-C. Zhang, J.-X. Wang, B. Jia, Z.-Y. Gao, and Q.-S. Wu, *Theoretical analysis of a hybrid traffic model accounting for safe velocity*, Mod. Phys. Lett. B **31**(2017): 1750104.
[46] Z. Wang, R. Cheng, and H. Ge, *Nonlinear analysis of an improved continuum model considering mean-field velocity difference*, Phys. Lett. A **383**(2019), 622–629.
[47] Z. Wang and W.-X. Zhu, *Modeling and stability analysis of traffic flow considering electronic throttle dynamics on a curved road with slope*, Physica A Stat. Mech. Appl. **597**(2022): 127225.
[48] S. Wolfram, *Statistical mechanics of cellular automata*, Rev. Mod. Phys. **55**(1983), 601–644.
[49] K. Zavitsas, I. Kaparias, M. G. H. Bell, and M. Tomassini, *Transport problems in cities*, Isis **6**(2010): 05.
[50] C. Zhai and W. Wu, *A continuum model considering the uncertain velocity of preceding vehicles on gradient highways*, Physica A Stat. Mech. Appl. **588**(2022): 126561.
[51] W. H. Ai, J. Zhu, Y. Zhang, M. Wang and D. W. Liu, *Bifurcation control analysis based on continuum model with lateral offset compensation*, Phys. A 624 (2023): 128961.

G. O. Fosu, corresponding author, Department of Mathematics, Kwame Nkrumah University of Science and Technology, Kumasi, Ghana
Current address: same
Email address: gabriel.of@knust.edu.gh

D. Anokye, Department of Mathematics, Kwame Nkrumah University of Science and Technology, Kumasi, Ghana
Email address: archimedesanokye123@gmail.com

A. Adu-Sackey, Department of Applied Mathematics, Koforidua Technical University, Ghana
Email address: albert.adu-sackey@ktu.edu.gh

B. E. Owusu, Department of Mathematics, Kwame Nkrumah University of Science and Technology, Kumasi, Ghana
Email address: bright.owusu@knust.edu.gh